

See discussions, stats, and author profiles for this publication at: <https://www.researchgate.net/publication/236662591>

# Ultrasonic guided wave propagation across waveguide transitions: Energy transfer and mode conversion

Article in *The Journal of the Acoustical Society of America* · May 2013

DOI: 10.1121/1.4795805 · Source: PubMed

CITATIONS

30

READS

710

5 authors, including:



**Jose Galan**

Universidad de Sevilla

11 PUBLICATIONS 288 CITATIONS

[SEE PROFILE](#)



**Baiyang Ren**

Pennsylvania State University

22 PUBLICATIONS 331 CITATIONS

[SEE PROFILE](#)



**Cliff Lissenden**

Pennsylvania State University

212 PUBLICATIONS 2,414 CITATIONS

[SEE PROFILE](#)

Some of the authors of this publication are also working on these related projects:



Directional nonlinear guided wave mixing in plate [View project](#)



Structural Health Monitoring of Composite Adhesive Bond [View project](#)

# Ultrasonic guided wave propagation across waveguide transitions: Energy transfer and mode conversion

Padmakumar Puthillath<sup>a)</sup>

212 Engineering Science and Mechanics, Pennsylvania State University, University Park, Pennsylvania 16802

Jose M. Galan

Escuela Superior de Ingenieros, Universidad de Sevilla, Camino de los Descubrimientos s/n, E-41092, Sevilla, Spain

Baiyang Ren, Cliff J. Lissenden, and Joseph L. Rose

212 Engineering Science and Mechanics, Pennsylvania State University, University Park, Pennsylvania 16802

(Received 3 December 2012; accepted 28 February 2013)

Ultrasonic guided wave inspection of structures containing adhesively bonded joints requires an understanding of the interaction of guided waves with geometric and material discontinuities or transitions in the waveguide. Such interactions result in mode conversion with energy being partitioned among the reflected and transmitted modes. The step transition between an aluminum layer and an aluminum-adhesive-aluminum multi-layer waveguide is analyzed as a model structure. Dispersion analysis enables assessment of (i) synchronism through dispersion curve overlap and (ii) wavestructure correlation. Mode-pairs in the multi-layer waveguide are defined relative to a prescribed mode in a single layer as being synchronized and having nearly perfect wavestructure matching. Only a limited number of mode-pairs exist, and each has a unique frequency range. A hybrid model based on semi-analytical finite elements and the normal mode expansion is implemented to assess mode conversion at a step transition in a waveguide. The model results indicate that synchronism and wavestructure matching is associated with energy transfer through the step transition, and that the energy of an incident wave mode in a single layer is transmitted almost entirely to the associated mode-pair, where one exists. This analysis guides the selection of incident modes that convert into transmitted modes and improve adhesive joint inspection with ultrasonic guided waves.

© 2013 Acoustical Society of America. [http://dx.doi.org/10.1121/1.4795805]

PACS number(s): 43.35.Cg, 43.20.Mv [JAT]

Pages: 2624–2633

## I. INTRODUCTION

Ultrasonic guided waves enable structural health monitoring and nondestructive evaluation of inaccessible adhesively bonded joints that would otherwise be impossible to inspect, or would require significant disassembly to provide access to the joint. They enable monitoring or testing to be performed in an efficient manner since a relatively large area can be monitored from one setup. However, these multi-mode waves typically must be transmitted across transitions in the waveguide. Selecting incident modes that are converted to propagating modes in the second waveguide is a significant challenge that once met should improve signal to noise ratios and defect sensitivity. Herein, our objective is to show that dispersion analysis is able to guide selection of incident modes that are transmitted through a discrete waveguide transition. Nearly ideal transmission is expected for special mode-pairs (which will be defined) that have highly correlated wavestructures and synchronism. Thus, incident and transmitted modes with overlapping dispersion curves and matching wavestructures are sought. Since dispersion analysis is not able to actually predict transmission across a transition, a model is developed for that purpose.

The geometry analyzed is that of a discontinuous layer adhesively bonded to a continuous layer as shown in the cross-sectional view of Fig. 1. Our nomenclature is that layer 1 is continuous, layer 2 is discontinuous, the waveguide transition occurs at  $x_1 = x_0$ , and the waveguides on either side of the transition are denoted  $A$  ( $x_1 < x_0$ ) and  $B$  ( $x_1 > x_0$ ). Guided wave propagation in the positive  $x_1$  direction is considered. While the end goal is to monitor the adhesive joint in waveguide  $B$ , the scope of this paper is limited to mode conversion and energy transmission through the waveguide transition as a necessary step toward the end goal.

Relative to the literature on adhesive bond characterization, the literature on guided wave transmission across a transition region is limited. Rokhlin (1991) used the Wiener-Hopf technique for analytical study of the interaction of Lamb-type waves with the transition in adhesive joints. The following studies relied on hybrid approaches that combined analytical and numerical methods to understand guided wave interaction with a transition (Chang and Mal, 1995; Ditri, 1996; Lowe *et al.*, 2000; Demma *et al.*, 2003; Lanza di Scalea *et al.*, 2004; Song *et al.*, 2005; Puthillath *et al.*, 2007; Puthillath *et al.*, 2008).

Chang and Mal (1995) used a combination of finite elements (FE) at the transition and global functions to represent wave propagation away from the transition, and a global-local FE method to study guided wave mode conversion and

<sup>a)</sup>Author to whom correspondence should be addressed. Electronic mail: kumarpp@gmail.com

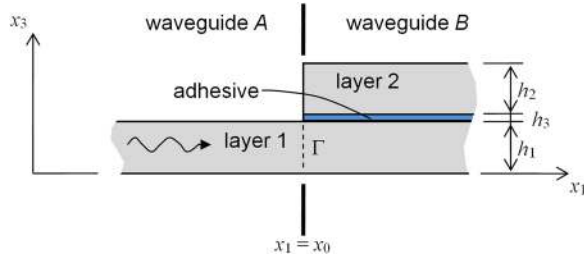


FIG. 1. (Color online) The transition between single layer waveguide A and multi-layer waveguide B occurs at  $x_1 = x_0$ . Wave propagation is in the  $x_1$  direction.

reflection/transmission aspects. Ditre (1996) studied the interaction of shear-horizontal (SH) waves at an abrupt change in an isotropic layer using a collocation technique. A very important contribution by Ditre is the mathematical foundation of the coupling/noncoupling of SH wave modes at waveguide transitions based on the orthogonality of the displacement fields in the waveguides forming the transition region. According to Ditre, any mode in the secondary waveguide whose displacement field distribution is orthogonal to the displacement field distribution of the incident mode will not be generated by the incident mode. Later, Demma *et al.* (2003) applied FE and modal decomposition to study SH wave interaction with a step discontinuity. Lowe *et al.* (2000) performed an elaborate FE analysis to understand the mode conversion and transmission of Lamb modes across an adhesive step-lap joint along with the influence of the bond geometry for  $s_0$  mode incidence. They used a two-dimensional Fourier transform technique to analyze the mode conversion aspects associated with the step transition in the lap joint. They observed that a higher energy is carried by the first order modes in the bond region and explain it in terms of wavestructures. Lanza di Scalea *et al.* (2004) complimented the work of Lowe *et al.* (2000) by experimentally studying the transmission of the  $a_0$  mode across an aluminum step-lap joint. The wavestructure based explanation to mode conversion parallels that of Lowe *et al.* (2000). They observed that the fundamental modes in the bond region play a major role in energy transfer from an  $a_0$  mode incidence at the joint.

Matt *et al.* (2005) also studied the wave propagation along and across a cross-ply composite spar attached to a quasi-isotropic skin using one-dimensional semi-analytical finite element (SAFE) based calculations. They found the most sensitive point for inspection to be the location where mode coupling occurred between the fundamental symmetric and the first order antisymmetric mode in the bonded region of the joint. This results in a larger interlayer energy transfer. They employed the ratio of the power flow in a subset of the total number of layers to the total cross-sectional power flow in order to determine the strength of energy transmission for different bond conditions. Song *et al.* (2005) developed a hybrid approach combining FE and boundary elements to study the guided wave mode conversion at a step-lap welded steel connection. From a parametric study varying the overlap length, they observed that the incident mode, frequency range, and overlap length all influence the transmission and reflection of guided waves. A hybrid FE technique to

compute mode conversion and scattering at a bonded joint transition and a parametric study along the same lines were performed by Puthillath *et al.* (2007) and Puthillath *et al.* (2008).

The body of this paper first summarizes the fundamental dispersion analysis for guided waves in a traction-free multi-layer (Sec. II) and then extends that analysis to the correlation of wavestructures as well as defines and investigates mode-pairs (Sec. III). As mode-pairs satisfy the displacement continuity conditions at the waveguide transition, nearly all the energy in the incident mode is expected to be transferred to the mode pair. Section IV presents a hybrid model that couples SAFE analysis with the normal mode expansion (NME) to show that wavestructure matching, and mode-pairs in particular, do correlate with energy transfer through the transition. Model predictions are compared with the dispersion analysis in Sec. V, and then conclusions are drawn.

## II. DISPERSION ANALYSIS

Wave propagation within a single layer (e.g., layer 1 in waveguide A shown in Fig. 1) is governed by Navier's equation of motion

$$(\lambda + \mu)u_{j,ij} + \mu u_{i,jj} = \rho \ddot{u}_i, \quad (1)$$

where  $\lambda$  and  $\mu$  are Lamé's constants,  $\rho$  is mass density, and  $u$  is the displacement. Traction-free boundary conditions for waveguide A are  $T_i(x_3 = 0, h_1) = 0$ . For the multi-layer plate in waveguide B, Eq. (1) holds for each layer and the traction-free boundary conditions are  $T_i(x_3 = 0, h_1 + h_3 + h_2) = 0$ . The continuity equations must also be satisfied between the layers in waveguide B,

$$u_i(x_3 = h_1)|_{\text{layer 1}} = u_i(x_3 = h_1)|_{\text{adhesive}}, \quad (2a)$$

$$T_i(x_3 = h_1)|_{\text{layer 1}} = T_i(x_3 = h_1)|_{\text{adhesive}}, \quad (2b)$$

$$u_i(x_3 = h_1 + h_3)|_{\text{layer 2}} = u_i(x_3 = h_1 + h_3)|_{\text{adhesive}}, \quad (2c)$$

$$T_i(x_3 = h_1 + h_3)|_{\text{layer 2}} = T_i(x_3 = h_1 + h_3)|_{\text{adhesive}}. \quad (2d)$$

The dispersion analysis takes the waveguide cross-section to be prismatic (Auld, 1990; Rose, 1999). Thus, dispersion analyses of waveguides A and B must be performed separately. Presuming that layers 1 and 2 are aluminum and the adhesive is epoxy with the parameters given in Table I, the dispersion curves for both waveguides A and B are shown in Fig. 2. Dashed and solid lines represent waveguides A and B, respectively, in both the phase velocity and group velocity dispersion curves. The modes in A are labeled as antisymmetric ("a") or symmetric ("s") with a numeric subscript.

TABLE I. Waveguide parameters.

Material	Thickness (mm)	Density (kg/m <sup>3</sup> )	Young's modulus (GPa)	Poisson's ratio
Aluminum	2	2700	69.43	0.33
Epoxy	0.3	1104	2.56	0.40
Titanium	2	4430	111	0.31

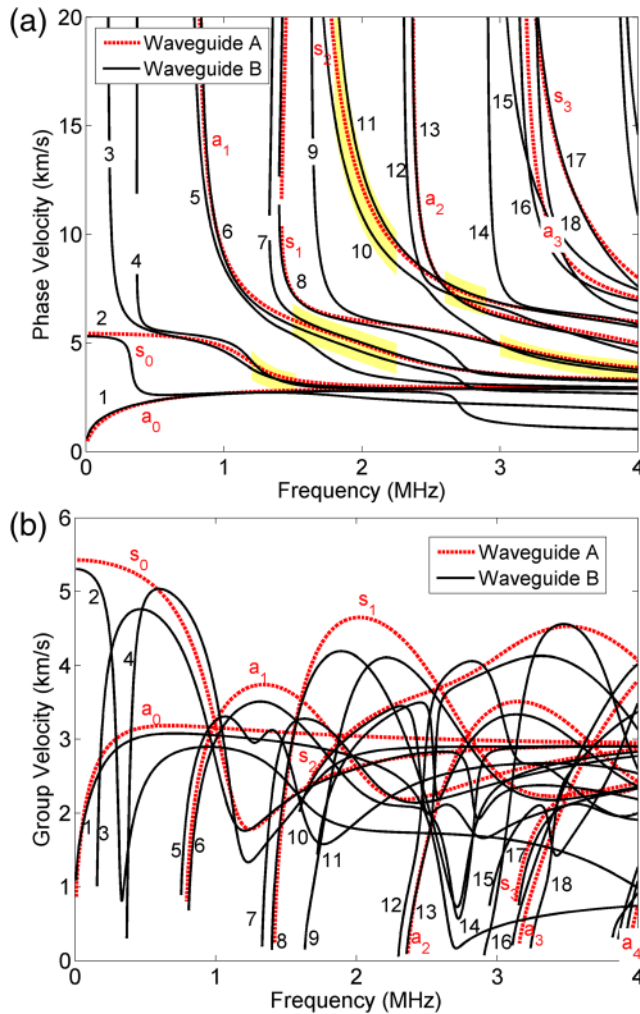


FIG. 2. (Color online) Superimposed (a) phase velocity and (b) group velocity dispersion curves for waveguides A and B.

The modes in B are incrementally numbered for generality and to avoid confusion.

Close examination of the phase velocity dispersion curves in Fig. 2(a) reveals certain frequency ranges where two modes for B nearly lay over those for A. Five such domains are highlighted in Fig. 2. These modes within B are termed a “mode-pair” for that particular mode in A. A formal wavestructure-based definition for a mode-pair is provided in Sec. III. An example mode-pair for mode  $s_2$  in A is modes 10 and 11 in B within the 1.73–2.33 MHz frequency range. Not only do the phase velocity dispersion curves match within this frequency range, but to a lesser degree so do the group velocity curves [see Fig. 2(b)]. It is easy to find regions other than the five marked in Fig. 2(a) where dispersion curves for waveguides A and B match, and this will be commented on in Sec. III.

The wavestructures of the  $s_2$  mode in A and the mode-pair 10-11 in B at 1.98 MHz are shown in Fig. 3. Remarkably, the displacement profiles within layer 1 are nearly identical for all three modes; this is discussed with respect to displacement continuity conditions in Sec. III. Since the mode in the primary waveguide is symmetric, the in-plane displacement ( $u_1$ ) distributions in layer 1 for mode-pair 10-11 are nearly symmetric while the out-of-plane

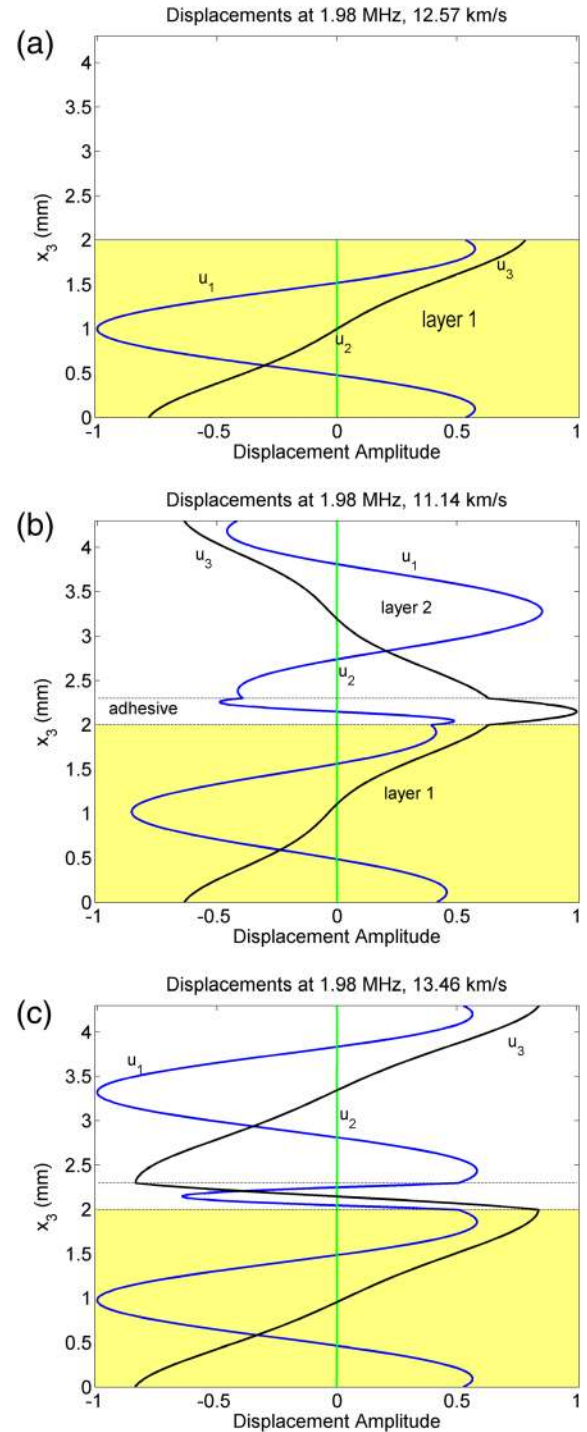


FIG. 3. (Color online) Displacement wavestructures at 1.98 MHz for (a)  $s_2$  mode in A, (b) mode 10 in B, and (c) mode 11 in B.

displacement ( $u_3$ ) distributions are antisymmetric. The in-plane displacement distributions in layer 2 are  $-1.0\times$  and  $+1.0\times$  their counterparts in layer 1 for modes 10 and 11, respectively. Thus, the in-plane displacement distribution in the adhesive is antisymmetric for mode 10 and symmetric for mode 11. Overall, mode 10 is antisymmetric while mode 11 is symmetric. Notice that the in-plane displacement at the interface between layer 1 and the adhesive is quite large for both modes 10 and 11. Further, the in-plane displacement gradient through the thickness of the adhesive is severe for

both modes 10 and 11. These wavestructure features are advantageous for monitoring adhesive integrity.

The source of mode-pair formation appears to be related to the symmetry limitations of wave modes for the waveguide. The existence of mode-pairs in  $B$  and their special features with respect to the phase and group velocity matching and similarity in wavestructure with the corresponding mode in  $A$  is expected to be very useful for mode selection. Wavestructure correlation is assessed quantitatively and used to formally define a mode-pair in Sec. III.

### III. ADDITIONAL DISPERSION ANALYSIS: CORRELATION AND MODE-PAIRS

A mode in waveguide  $A$  having a wavestructure that matches that in waveguide  $B$  in the connected subdomain ( $\Gamma$  in layer 1) is intuitively expected to ensure efficient transfer of energy across the transition (Auld, 1990; Lowe *et al.*, 2000; Lanza di Scalea *et al.*, 2004; Matt *et al.*, 2005). Thus, we seek modes in  $B$  that have nearly identical wavestructure in layer 1. In other words, we seek to satisfy the displacement continuity conditions between waveguides  $A$  and  $B$  at  $x_1 = x_0$  for the incident mode in  $A$  with a mode or mode-pair in  $B$ . In this way, additional modes in  $B$  are not required to satisfy the continuity conditions, and maximum energy will be transferred from the incident mode in  $A$  to the mode or mode-pair in  $B$ . Note, however, that traction continuity at  $x_1 = x_0$  is not specifically addressed.

Wavestructure matching is assessed by establishing a correlation coefficient, similar in name to that employed by Matt *et al.* (2005). The correlation between two vectors is their covariance normalized with respect to the product of their standard deviations. High correlation does not necessarily mean that the vectors are identical, but rather that they are scalable. A wavestructure matching coefficient,  $\rho_{A_i B_j}|_{f, \Gamma}$ , is defined here for frequency  $f$  as the summation of the correlation between the components of the wavestructure of the  $i$ th mode in waveguide  $A$  to the wavestructure of the  $j$ th mode in waveguide  $B$  over the length of the connected region  $\Gamma$  defined by  $x_1 = x_0$ ,  $0 \leq x_3 \leq h_1$ . It is mathematically expressed as

$$\rho_{A_i B_j}|_{f, \Gamma} = \sum_{k=1}^3 \frac{\text{cov}(u_k^{A_i}, u_k^{B_j})}{\sigma_{A_i} \sigma_{B_j}}, \quad (3)$$

where  $\text{cov}$  and  $\sigma$  represent covariance and standard deviation, respectively.

The covariance can be shown to be an alternate means of expressing the orthogonality of the wavestructures, which is a check for guided wave mode coupling developed by Ditre (1996) for SH waves. Here,  $\rho_{AB} = 0$  for fully decoupled modes. Additionally,  $\rho_{AB}$  satisfies reciprocity as a consequence of the commutative property of each term in  $\rho_{AB}$ . Employing the normality of the guided wave modes, the contribution of each mode at a prescribed frequency normalized with respect to all possible modes at that frequency is an indicator of the energy partitioning among modes. The partitioned expression of the wavestructure matching coefficient is obtained by normalizing with respect to all modes in waveguide  $B$ ,

$$\rho_{A_i B_j}^p|_{f, \Gamma} = \frac{\rho_{A_i B_j}|_{f, \Gamma}}{\sum_{j=1}^{N_B} \rho_{A_i B_j}|_{f, \Gamma}}. \quad (4)$$

The partitioned wavestructure matching coefficient for the incident  $s_1$  mode from waveguide  $A$  to  $B$  is shown in Fig. 4. The coefficient is clearly high where the phase velocity dispersion curves overlap, suggesting that the incident mode will get mode converted to the overlapped mode in  $B$  resulting in strong energy transfer across the transition. The  $s_1$  mode overlaps modes in  $B$  for much of its length, but  $\rho_{AB}^p$  is highest between 3–4 MHz where the overlap is with modes 9 and 10, which we will soon show to be a mode-pair. The other overlapping lengths are with a single mode: mode 8 in the highly dispersive region, and then mode 9. It is important to point out that dispersion curve overlap is not necessary for wavestructure correlation as indicated by modes 3 and 4 at 1.5 MHz in Fig. 4. However, we will see in Sec. IV that wavestructure correlation without dispersion curve overlap (i.e., synchronism) does not lead to strong energy transfer.

Wavestructure correlation can be taken a step further and used to formally define a mode-pair. To this end, we define a mode-pair as two modes in waveguide  $B$  that each has a nearly perfect correlation coefficient, i.e., they each match the wavestructure in waveguide  $A$ . Since Lamb-like wave modes do not have displacement components in the  $x_2$  direction, perfectly matched wavestructures have a correlation coefficient  $\rho_{AB} = 2.0$ . A value of 1.9 has been selected to represent “nearly perfect” matching. This definition was used to distinguish the mode-pairs highlighted in Fig. 2(a) from other regions having overlapping dispersion curves but not correlated wavestructures.

The mode-pairs 3-4, 6-7, 9-10, and 10-11 for incident modes  $s_0$ ,  $a_1$ ,  $s_1$ , and  $s_2$ , respectively, are shown in Figs. 5–8. Figure 2(a) shows that five mode-pairs occur for the first eight incident modes in  $A$ . Details are provided for four of these five sets of mode-pairs to show that each case is unique. The mode-pair not shown is 11-12 for the  $s_2$  incident

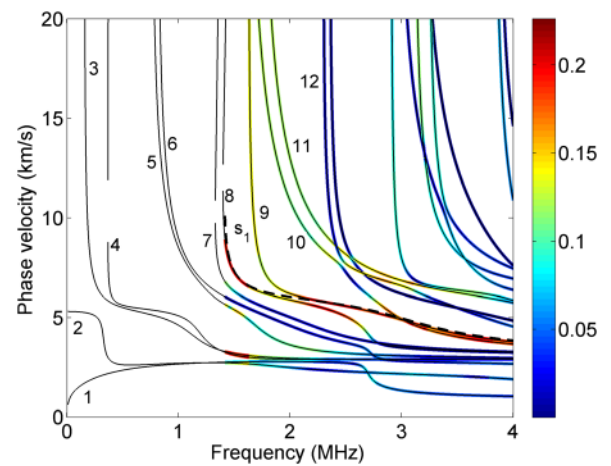


FIG. 4. (Color online) Partitioned wavestructure correlation coefficient superimposed on dispersion curves for waveguide  $B$  given an incident  $s_1$  mode in  $A$ . The incident  $s_1$  mode dispersion curve is dashed.

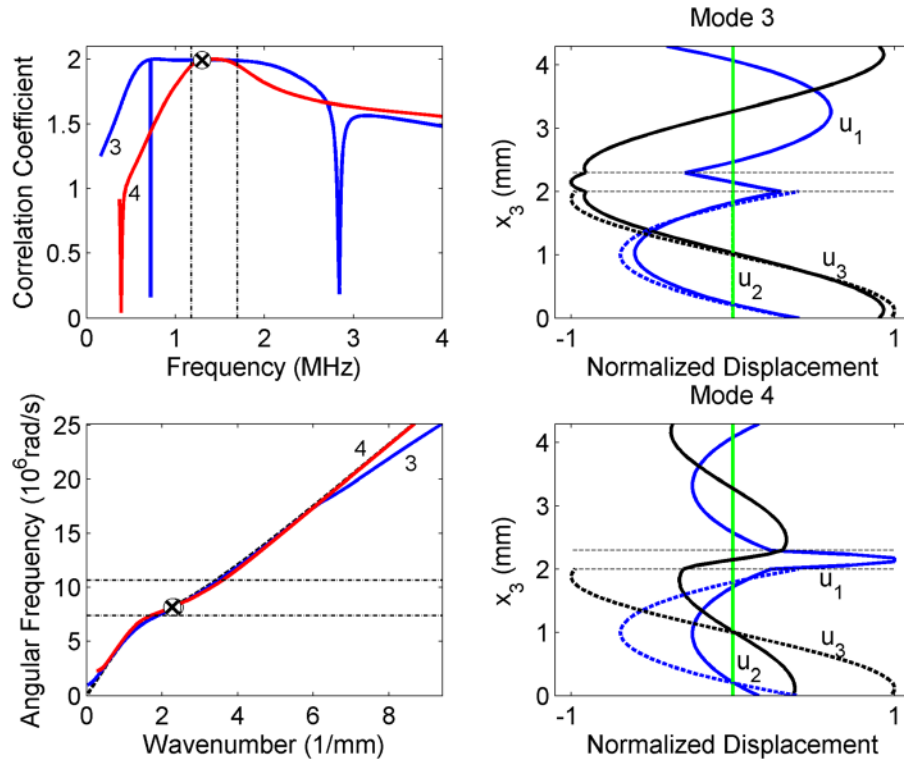


FIG. 5. (Color online) Mode-pair 3-4 for incident mode  $s_0$ . The correlation coefficients (top-left), dispersion curve overlap (bottom-left), and the wavestructure at 1.30 MHz (right column). The incident mode is shown with dashed lines in the dispersion curve overlap and the wavestructure plots.

mode for approximately 2.6–2.9 MHz. Each of Figs. 5–8 has three components.

- (i) The correlation coefficients  $\rho_{AB}$  for the mode pair are plotted as a function of frequency. This plot enables the frequency range over which the mode-pair exists to be determined. Mode-pairs are defined to have nearly perfect correlation coefficients  $\rho_{AB} \geq 1.9$ . The dotted-dashed vertical lines mark the frequency range

of the mode pair. A symbol marks the frequency for which wavestructures are plotted. Obviously, there is no correlation coefficient below the cutoff frequency if one exists.

- (ii) The  $\omega$ - $k$  dispersion curves for the mode-pair and the incident mode are plotted, where  $\omega = 2\pi f$  is the angular frequency and  $k = \omega/c_p$  is the wavenumber. Since the group velocity is defined to be  $c_g = d\omega/dk$ ,  $\omega$ - $k$

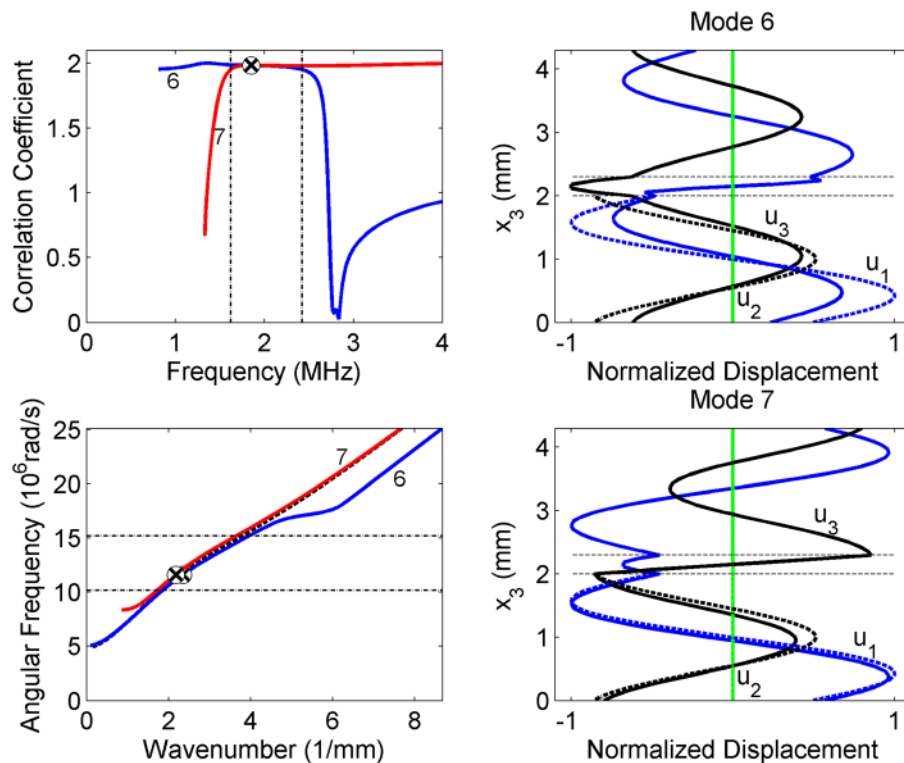


FIG. 6. (Color online) Mode-pair 6-7 for incident mode  $a_1$ . The correlation coefficients (top-left), dispersion curve overlap (bottom-left), and the wavestructure at 1.85 MHz (right column). The incident mode is shown with dashed lines in the dispersion curve overlap and the wavestructure plots.

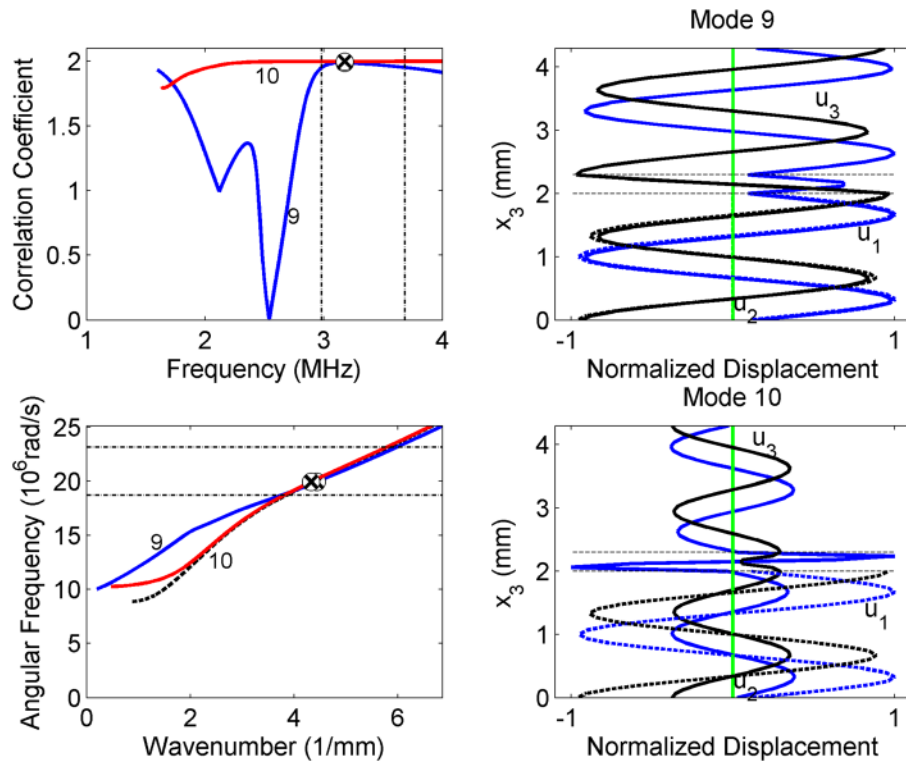


FIG. 7. (Color online) Mode-pair 9-10 for incident mode  $s_1$ . The correlation coefficients (top-left), dispersion curve overlap (bottom-left), and the wavestructure at 3.18 MHz (right column). The incident mode is shown with dashed lines in the dispersion curve overlap and the wavestructure plots.

dispersion curves show both phase velocity matching (at intersection points) and group velocity matching (identical slopes). The incident mode is shown with a dashed line, and the frequency range of the mode-pair and the wavestructure point are also marked.

- (iii) The wavestructures for the mode-pair at the specified frequency are shown along with the wavestructure for the incident mode (dashed lines). These figures show that the nearly perfect matching of a mode-pair

indicates that they have the same shape in the  $\Gamma$  sub-domain. Because wavestructures are eigenvectors that represent the shape of the displacement profile, only shape correlation is necessary and absolute values are insignificant. As already mentioned, the displacement  $u_2$  is always zero.

The top-left plots in Figs. 5–8 indicate that the correlation coefficient can change quite rapidly with frequency,

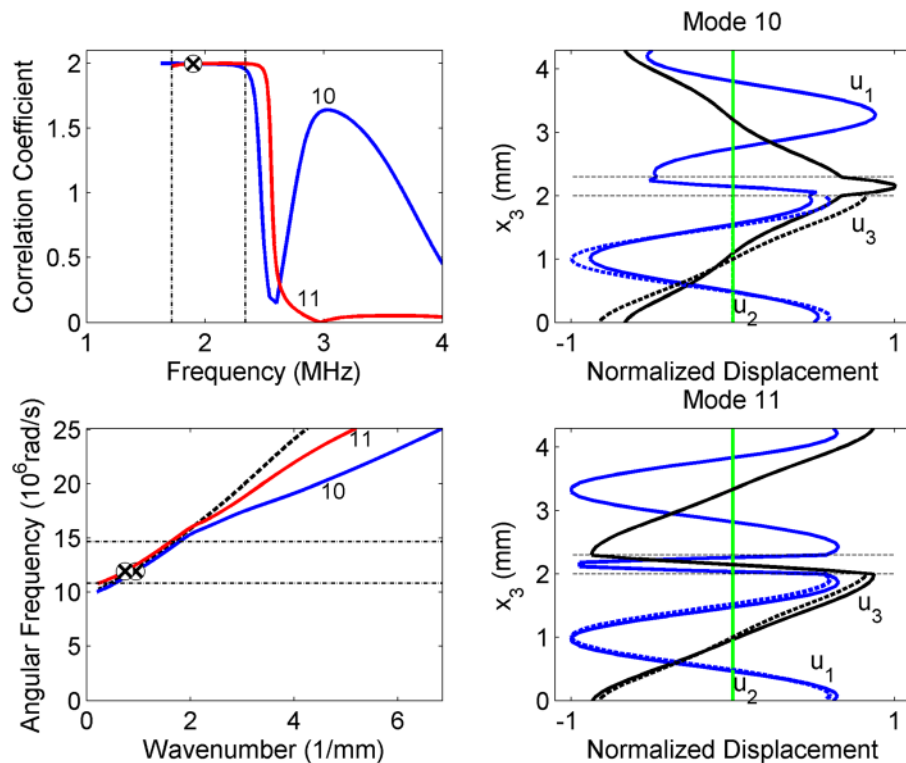


FIG. 8. (Color online) Mode-pair 10-11 for incident mode  $s_2$ . The correlation coefficients (top-left), dispersion curve overlap (bottom-left), and the wavestructure at 1.90 MHz (right column). The incident mode is shown with dashed lines in the dispersion curve overlap and the wavestructure plots.

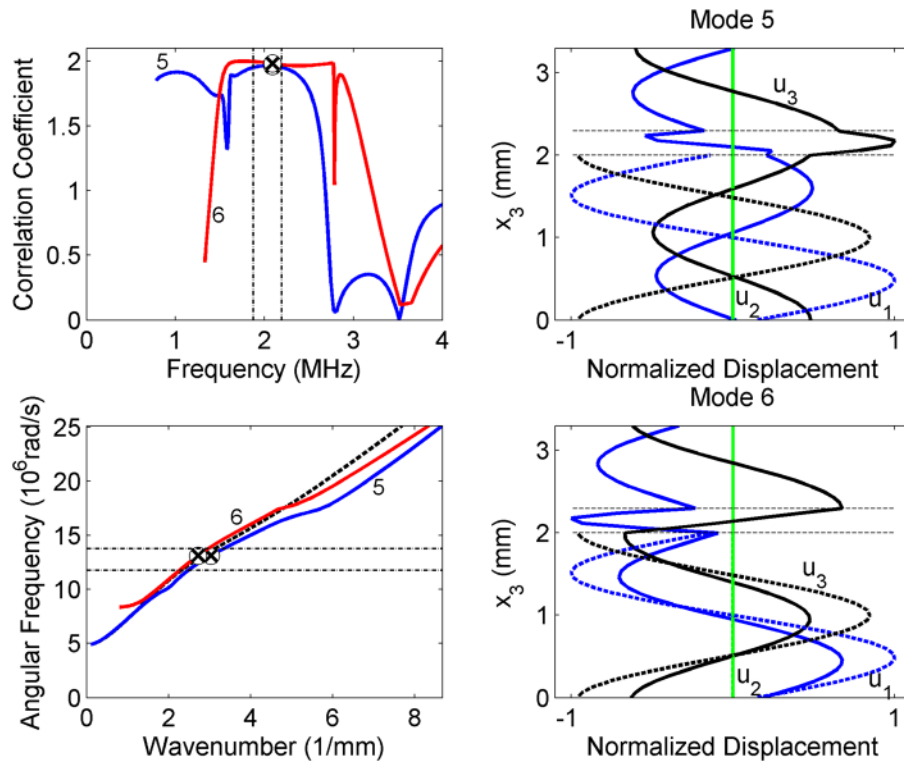


FIG. 9. (Color online) 1-mm thick aluminum layer 2. Mode-pair 5-6 for incident mode  $a_1$ . The correlation coefficients (top-left), dispersion curve overlap (bottom-left), and the wavestructure at 2.09 MHz (right column). The incident mode is shown with dashed lines in the dispersion curve overlap and the wavestructure plots.

demonstrating that the wavestructure for a prescribed mode can change abruptly with frequency. Outside of the mode-pair frequency domain one mode may have a stronger wavestructure correlation than the other (i.e., mode 3 relative to mode 4 in Fig. 5, and mode 10 relative to mode 9 in Fig. 7), or one mode may match at lower frequencies while the other matches better at higher frequencies (i.e., modes 6 and 7 in Fig. 6), or it could be that neither mode matches well (i.e., modes 10 and 11 in Fig. 8). Within the mode-pair

domain synchronism of both phase and group velocities occurs as shown at the bottom-left in Figs. 5–8. However, outside of the mode-pair domain there is typically a mismatch in phase or group velocity of one or both of the modes in waveguide  $B$  relative to the incident mode in  $A$ . The exception to this general rule is mode-pair 3-4 for incident mode  $s_0$  (Fig. 5), where dispersion curve overlap occurs for approximately 0.5–2.9 MHz, but the mode-pair subdomain is only 1.2–1.7 MHz. The right column in Figs.

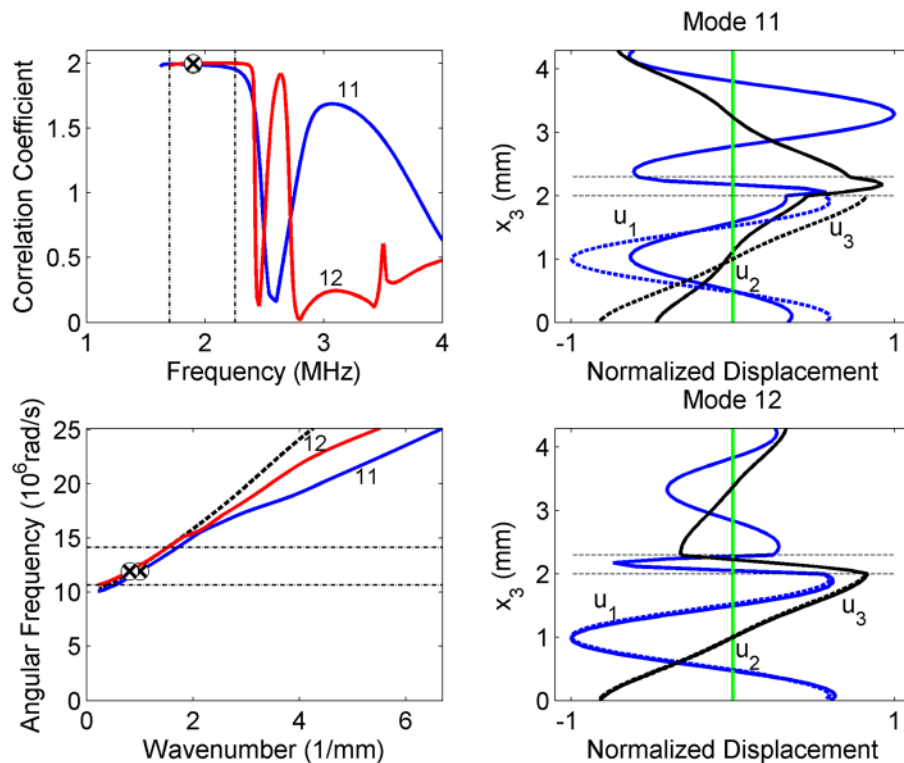


FIG. 10. (Color online) 2-mm thick titanium layer 2. Mode-pair 11-12 for incident mode  $s_2$ . The correlation coefficients (top-left), dispersion curve overlap (bottom-left), and the wavestructure at 1.90 MHz (right column). The incident mode is shown with dashed lines in the dispersion curve overlap and the wavestructure plots.

5–8 show that the shapes of the displacement profiles in layer 1 match very well, as required by the high correlation coefficient. In layer 2, the shape of the displacement profiles are mirror images. Furthermore, in the adhesive the in-plane displacement component has a large gradient, which is beneficial for defect monitoring in the adhesive. The location of the peak in-plane displacement in the adhesive is mode-dependent, which illustrates the importance of proper mode selection.

The waveguide transition studied up to this point is quite simple because the bonded joint is symmetric about its midplane as shown in Fig. 1, which brings up the question of whether mode-pairs are present at transitions where waveguide *B* is not symmetric about the midplane. Thus, two variations to the joint shown in Fig. 1 are considered. (i) The thickness of layer 2 is reduced from 2 mm to 1 mm. (ii) The layer 2 material is changed from aluminum to titanium (see Table I).

Figure 9 shows the mode-pair 5-6 for incident mode  $a_1$  and a 1 mm thick aluminum layer 2. This is the only mode-pair that exists, although some modes in waveguide *B* are well correlated to modes in waveguide *A*. The right column in Fig. 9 indicates that the displacement profiles in layer 2 also match well, while those in the adhesive do not. On the other hand, if layer 2 is 2 mm thick titanium, then mode-pairs very similar to those shown in Figs. 5–8 exist. The mode-pair 11-12 for incident mode  $s_2$  is shown in Fig. 10. In this case, the mode-pair exists close to the cutoff frequency.

While the correlation of wavestructures leads us to believe that satisfying the displacement continuity conditions across  $\Gamma$  at the waveguide transition will result in strong energy transfer, we seek proof. A model is presented in Sec. IV that predicts mode conversions and energy transfer.

#### IV. HYBRID MODE CONVERSION MODEL

Analysis at a discrete transition to determine transmitted and reflected modes can demonstrate whether the wavestructure matching and mode-pair concepts are correlated with mode conversion and energy transfer. A hybrid model combining SAFE analysis and the NME is developed and applied to analyze the wave scattering at a waveguide transition.

The SAFE framework, as developed in Galan and Abascal (2002), Hayashi *et al.* (2003), and several other publications, has tremendous advantages in handling guided wave propagation across complex cross-sections having a prismatic geometry. Essentially, SAFE analysis employs an exponential propagating term to represent the wave propagation along the waveguide and a FE discretization of the cross-section. The fundamental equations for SAFE analysis are based on the same principles as FE. At each frequency, a quadratic eigensystem is obtained whose solution provides the dispersion curves and modal wavestructures. The NME assumes the completeness of guided wave modes, i.e., any displacement can be expressed in terms of the displacement wavestructures of the modes present in the waveguide at that frequency (Kirmann, 1995).

SAFE analysis is coupled with the NME here in order to predict guided wave mode conversion at waveguide transitions. Considering wave propagation as a plane strain

problem, evaluation of mode conversion at a waveguide transition is reduced to the analysis of the interface between waveguides *A* and *B* ( $x_1 = x_0$ ). The common cross-sectional line at the transition is discretized into quadratic elements. For convergence of the solution, the dimension of the quadratic elements ( $L_e$ ) in every material layer is calculated using (Galan and Abascal, 2002)

$$L_e = \frac{1}{4} \left( \frac{2\pi c_T}{\omega_{\max}} \right), \quad (5)$$

where  $c_T$  is the transverse wave speed and  $\omega_{\max}$  is the maximum angular frequency. Equation (5) simply indicates that there should be at least four quadratic elements per shear wavelength.

The framework provided by Cho and Rose (1996), Rose (1999), Galan and Abascal (2002), and Song *et al.* (2005) enables determination of mode converted reflected and transmitted waves from an incident wave in waveguide *A*. A single mode incidence is simulated by providing the displacement and traction profiles to the nodes corresponding to the incident mode (a right propagating wave in waveguide *A*) at the common junction  $\Gamma$  in the transition (see Fig. 1). At the waveguide transition  $x_1 = x_0$ , the displacement and traction continuity conditions are imposed as are the traction-free conditions on the free surface. The resultant scattered displacement and stress profiles must satisfy

$$\left. \begin{aligned} u_i^I + u_i^R &= u_i^T \\ T_i^I + T_i^R &= T_i^T \end{aligned} \right\} 0 \leq x_3 \leq h_1$$

$$T_i^T = 0, \quad h_1 \leq x_3 \leq h_2 + h_3, \quad (6)$$

where the superscripts *I*, *R*, and *T* refer to the incident, reflected, and transmitted fields, respectively. In the SAFE analysis, the displacement continuity conditions are enforced exactly by using matching meshes at the junction and by setting equal the displacements of coincident nodes. On the other hand, the traction continuity is applied in a weak manner. By premultiplying the stresses by a virtual displacement and integrating over the cross-section consistent nodal forces are obtained, which are later used to write the equilibrium equations at each node.

At each frequency, the NME is applied to express the displacements and tractions in each waveguide in terms of all the possible modes existing in each of them. The modes calculated with SAFE analysis are used in the NME expansion

$$\sum_{m=1}^{N_j} \alpha(\omega)_j^m \phi_i(x_3, \omega)_j^m = u_i(x_3, \omega)_j;$$

$$\sum_{m=1}^{N_j} \alpha(\omega)_j^m \psi_i(x_3, \omega)_j^m = T_i(x_3, \omega)_j, \quad (7)$$

$m = 1, 2, \dots, N_j$  modes in waveguide *j* (calculated with SAFE),

$i = 1, 2, 3$  (directions),

$j = A, B$  (waveguides),

$\alpha(\omega)_j^m$  = amplitude coefficient of mode *m* in waveguide *j*,  
 $\phi_i(x_3, \omega)_j^m$  = Displacement of mode *m* along direction *i* in waveguide *j*,

$u_i(x_3, \omega)_j$  = Resultant displacement along direction  $i$  in waveguide  $j$ ,  
 $\psi_i(x_3, \omega)_j^m$  = Traction on plane normal to  $x_1$  in direction  $i$  of mode  $m$  in waveguide  $j$ ,  
 $T_i(x_3, \omega)_j$  = Resultant traction on plane normal to  $x_1$  in direction  $i$  in waveguide  $j$ .

Only wave modes carrying energy away from the junction (i.e., reflected or transmitted modes) are considered to be unknowns in the NME. Their coefficients are calculated by solving the linear system of equations which results from substituting the NME [Eq. (7)] into the continuity conditions [Eq. (6)].

The reflected and transmitted power can be determined from the stress and displacement fields using Poynting's vector calculations, enabling energy balance calculations to be performed. The total energy in the system, i.e., the sum of the reflected and the transmitted energy at any frequency, normalized by the energy of the incident mode should be equal to unity. Any deviation from the energy balance is a measure of the error in the calculation. Model results are provided in Sec. V.

## V. HYBRID MODEL RESULTS

The phase velocity dispersion curve for the  $s_1$  mode in A overlaps with several modes in B over different frequency ranges as shown in Fig. 2(a), which makes it a good example to show the relationship between dispersion curve overlap and energy transmission. The displacement and stress wavestructures for mode  $s_1$  incidence in waveguide A were input into the hybrid model following the procedure described in Sec. IV. The total energy transmitted from A to B ( $T_{AB}$ ) was partitioned among the modes in B and is shown in the form of an intensity map on the corresponding dispersion curves for B in Fig. 11. The intensity map clearly shows that the majority of the energy is transmitted through modes 8 and 9 in the 1.8–2.6 MHz frequency range and through modes 9 and 10 in the 2.8–4.0 MHz range. Between the cutoff frequency of the  $s_1$  mode and 1.7 MHz the transmitted energy is small, indicating that significant reflection occurs. The

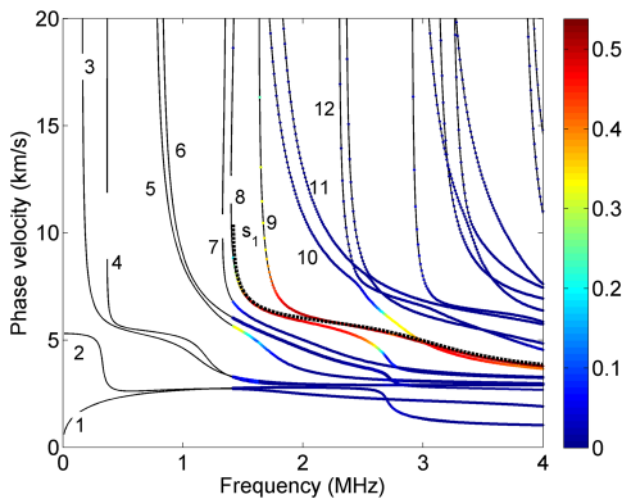


FIG. 11. (Color online) Intensity map of partitioning of the transmitted energy ( $T_{AB}$ ) among modes in waveguide B given  $s_1$  mode incidence from waveguide A.

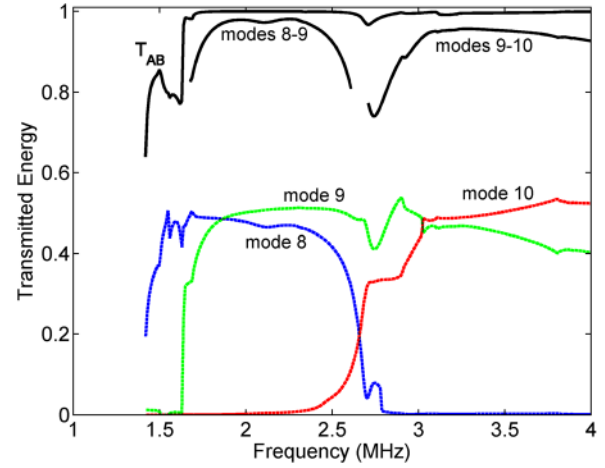


FIG. 12. (Color online) Transmitted energy for  $s_1$  mode incidence, total energy transmission  $T_{AB}$ , and contributions from combined modes 8, 9, and 10.

transmitted energy shown in Fig. 11 can be compared with the wavestructure matching shown in Fig. 4. Wavestructure matching agrees with transmitted energy where dispersion curves overlap the incident mode.

For the  $s_1$  incident mode the total energy transmission,  $T_{AB}$ , is shown in Fig. 12 as a function of frequency, along with the contributions to it from modes 8–10. It is clear from Fig. 12 that above 1.7 MHz almost all of the energy gets transmitted across the joint, as  $T_{AB}$  is between 0.95 and 1.0. Almost all of the transmitted energy occurs through modes 8 and 9 between 1.8–2.6 MHz, while modes 9 and 10 carry almost all of the transmitted energy between 2.8–4.0 MHz. A second example is shown in Fig. 13 for the  $s_2$  incident mode. Energy transferred to modes 10–14 is shown (dashed), as is energy transferred to mode-pair 10-11 over 1.7–2.4 MHz and mode-pair 12-13 over 2.6–2.9 MHz. Clearly, the highest energy transfer occurs in the domain of the mode-pair. As a third example, energy transfer from the  $s_0$  incident mode is shown in Fig. 14 for mode-pair 3-4.  $T_{AB}$  minima occur at 0.15 and 0.33 MHz, just before the cutoffs of modes 3 and 4 at 0.158 and 0.369 MHz, respectively. Physically, the minima occur due to divergence of the wavestructures for the incident  $s_0$  mode and modes 2 and 3. The

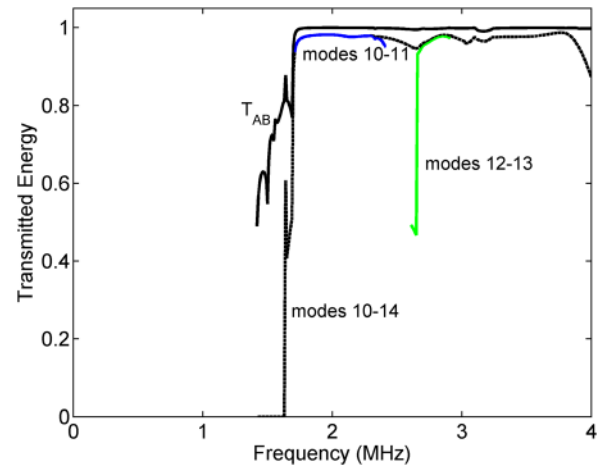


FIG. 13. (Color online) Transmitted energy for  $s_2$  mode incidence, total energy transmission  $T_{AB}$ , and contributions from mode-pairs 10-11 and 12-13.

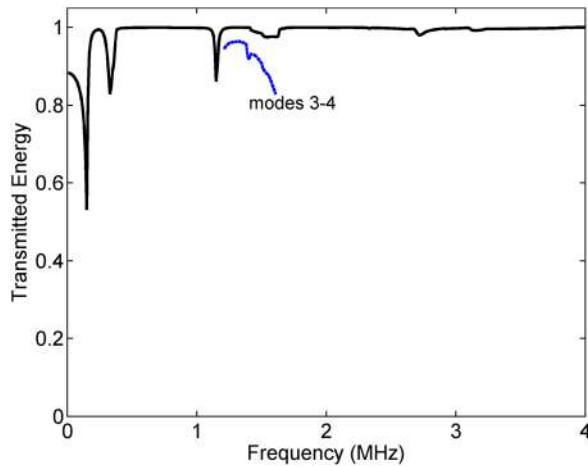


FIG. 14. (Color online) Transmitted energy for  $s_0$  mode incidence, total energy transmission  $T_{AB}$ , and contributions from mode-pair 3-4.

sharp increases in  $T_{AB}$  just after the minima occur because the wavestructures of the cutoff modes 3 and 4 correlate well with the incident mode. The energy transmission  $T_{AB}$  from 0–0.15 MHz is primarily through mode 2, but then transitions to modes 3 and 4 after their cutoffs. This corresponds to the overlapping dispersion curves  $s_0$ -2 for 0–0.15 MHz and  $s_0$ -3/ $s_0$ -4 above 0.5 MHz as shown in Fig. 2(a). As discussed in Sec. III, modes 3 and 4 form a mode-pair for 1.2–1.6 MHz, and there is a strong correlation between energy transmission and wavestructure matching. Moreover, overlapping dispersion curves that also exhibit wavestructure matching promote energy transmission.

In summary, mode-pairs in  $B$ , which by definition have nearly perfect wavestructure correlation with the incident mode in  $A$ , have nearly all the energy transferred from the incident mode in  $A$  to the mode-pair in  $B$ . Wavestructure correlation is a part of the dispersion analysis, while the computation of mode conversion and energy transfer requires an additional SAFE analysis and the NME.

## VI. CONCLUSIONS

In the ideal case of a discontinuous plate (layer 2) bonded to a continuous plate (layer 1), a discrete transition separates waveguide  $A$  (layer 1) from waveguide  $B$  (layer 1/adhesive/layer 2). Ultrasonic guided wave inspection of the adhesive joint typically requires energy transfer through the transition. Dispersion analysis of overlapping dispersion curves for waveguides  $A$  and  $B$  as well as matching wavestructures led to the discovery of mode-pairs where the wavestructures in layer 1 of the mode-pair in waveguide  $B$  are nearly identical to the wavestructure in waveguide  $A$ . These mode-pairs exist over finite frequency ranges. Five mode-pairs were found for equal thickness layers, but only one mode-pair was found if the layer thicknesses were different. A hybrid model employing SAFE analysis and the NME was developed and used to show that essentially all of the incident energy is transferred to mode-pairs where they exist. The model also confirms that matching wavestructures enable strong energy transfer from an incident mode in  $A$  to

a mode in  $B$  when the dispersion curves overlap, i.e., have synchronized phase and group velocities. Thus, it appears sufficient in this instance to identify correlated wavestructures by performing dispersion analysis, rather than having to create a separate mode conversion model.

The characteristics of mode-pairs in coupled waveguides, viz., higher energy transmission can be exploited in the inspection or monitoring of a host of adhesively bonded assemblies. The present analysis seems equally applicable to anisotropic waveguide assemblies. Additionally, it seems reasonable that by proper design of the waveguides and their transitions the transfer of ultrasonic energy across waveguide transitions can be enhanced or reduced to suit the application requirements.

## ACKNOWLEDGMENT

We gratefully acknowledge the support of the NASA Aircraft Aging and Durability Project under cooperative agreement number NNX07AB41A.

- Auld, B. A. (1990). *Acoustic Fields and Waves in Solids* (Krieger, Malabar, FL), pp. 1–421.
- Chang, Z., and Mal, A. K. (1995). “A global local method for wave propagation across a lap joint,” *Numerical Methods in Structural Mechanics, AMD (Am. Soc. Mech. Eng.)* **204**, 1–11.
- Cho, Y., and Rose, J. L. (1996). “A boundary element solution for a mode conversion study on the edge reflection of Lamb waves,” *J. Acoust. Soc. Am.* **99**, 2097–2109.
- Demma, A., Cawley, P., and Lowe, M. (2003). “Scattering of the fundamental shear horizontal mode from steps and notches in plates,” *J. Acoust. Soc. Am.* **113**, 1880–1891.
- Ditri, J. J. (1996). “Some results on the scattering of guided elastic SH waves from material and geometric waveguide discontinuities,” *J. Acoust. Soc. Am.* **100**, 3078–3087.
- Galan, J. M., and Abascal, R. (2002). “Numerical simulation of Lamb wave scattering in semi-infinite plates,” *Int. J. Numer. Methods Eng.* **53**, 1145–1173.
- Hayashi, T., Song, W.-J., and Rose, J. L. (2003). “Guided wave dispersion curves for a bar with an arbitrary cross-section, a rod and rail example,” *Ultrasonics* **41**, 175–183.
- Kirrmann, P. (1995). “On the completeness of Lamb modes,” *J. Elasticity* **37**, 39–69.
- Lanza di Scalea, F., Rizzo, P., and Marzani, A. (2004). “Propagation of ultrasonic guided waves in lap-shear adhesive joints: Case of incident  $a_0$  Lamb wave,” *J. Acoust. Soc. Am.* **115**, 146–156.
- Lowe, M. J. S., Challis, R. E., and Chan, C. W. (2000). “The transmission of Lamb waves across adhesively bonded lap joints,” *J. Acoust. Soc. Am.* **107**, 1333–1345.
- Matt, H., Bartoli, I., and Lanza di Scalea, F. (2005). “Ultrasonic guided wave monitoring of composite wing skin-to-spar bonded joints in aerospace structures,” *J. Acoust. Soc. Am.* **118**, 2240–2252.
- Puthillath, P., Kannajosyula, H., Lissenden, C. J., and Rose, J. L. (2008). “Ultrasonic guided wave inspection of adhesive joints: A parametric study for a step-lap joint,” in *Review of Progress in Quantitative Nondestructive Evaluation*, edited by D. O. Thompson and D. E. Chimenti (AIP, Melville, NY), Vol. 1096, pp. 1127–1133.
- Puthillath, P., Yan, F., Lissenden, C. J., and Rose, J. L. (2007). “Ultrasonic guided waves for the inspection of adhesively bonded joints,” in *Review of Progress in Quantitative Nondestructive Evaluation*, edited by D. O. Thompson and D. E. Chimenti (AIP, Melville, NY), Vol. 975, pp. 200–206.
- Rokhlin, S. I. (1991). “Lamb wave interaction with lap-shear adhesive joints: Theory and experiment,” *J. Acoust. Soc. Am.* **89**, 2758–2765.
- Rose, J. L. (1999). *Ultrasonic Waves in Solid Media* (Cambridge University Press, Cambridge), pp. 1–454.
- Song, W.-J., Rose, J. L., Galan, J. M., and Abascal, R. (2005). “Ultrasonic guided wave scattering in a plate overlap,” *IEEE Trans. Ultrason. Ferroelectr. Freq. Control* **52**, 892–903.